ORGANIC CHEMISTRY

Dearomative ring expansion of thiophenes by bicyclobutane insertion

Huamin Wang[1], Huiling Shao[2]†, Ankita Das[1]†, Subhabrata Dutta[1], Hok Tsun Chan[2], Constantin Daniliuc[1], K. N. Houk[2]*, Frank Glorius[1]*

Skeletal ring enlargement is gaining renewed interest in synthetic chemistry and has recently focused on insertion of one or two atoms. Strategies for heterocyclic expansion through small-ring insertion remain elusive, although they would lead to the efficient formation of bicyclic products. Here, we report a photoinduced dearomative ring enlargement of thiophenes by insertion of bicyclo[1.1.0]butanes to produce eight-membered bicyclic rings under mild conditions. The synthetic value, broad functional-group compatibility, and excellent chemo- and regioselectivity were demonstrated by scope evaluation and product derivatization. Experimental and computational studies point toward a photoredox-induced radical pathway.

Cyclic organic compounds, especially heterocycles, play a key role in pharmaceutical and natural products chemistry, as well as materials science (*1*–*3*). Ring architecture not only influences properties such as lipophilicity, three dimensionality, and scaffold rigidity but also determines molecular function and reactivity (*1*–*3*). Hence, the development of methods to precisely form and manipulate ring systems is of utmost importance in synthetic chemistry. Skeletal ring enlargement can convert common feedstocks into molecularly complex scaffolds and has the potential to induce important changes in the chemical or biological properties of the original compounds (*4*–*6*). Recently, the insertion of one or two atoms into cyclic molecules for skeletal editing, an approach first developed in 1881 (*7*), has received renewed attention (*8*–*16*). Notable contributions from several groups have been reported in the context of skeletal editing by means of boron (*10*), nitrogen (*11*, *12*), or carbon (*13*–*15*) atom insertion (Fig. 1A). Two-step approaches for dearomative ring enlargement of polycyclic arenes through insertion of oxygen (*17*) and carbon (*18*) have also been demonstrated. Moreover, catalytic strategies for two-atom insertions into highly strained cyclic carbonyls have emerged as a useful tool for the synthesis of bridged and fused rings (*19*) (Fig. 1A). Extending this concept to the insertion of small rings into a heterocyclic parent ring ("ring-in-a-heterocycle") would allow the facile construction of bicyclic frameworks (Fig. 1B).

The hetero(bi)cyclic moiety is the basic scaffold of numerous important biologically active natural products (*3*, *20*, *21*). Insertion of C(sp^3)-rich rings into heterocycles to form bicyclic compounds is appealing because sp^3 richness, three dimensionality, and increased conformational rigidity often facilitate the successful design of new drugs (*1*). From a synthetic perspective, bicyclo[1.1.0]butanes (BCBs) are ideal sources of C(sp^3)-rich rings because of their rigid and defined three-dimensional nature (*22*–*27*). The peripheral cyclization of unsaturated π-bonds with BCBs provides an approach to introduce bicyclic scaffolds in synthetic chemistry (*28*, *29*). Very recently, the cycloaddition of BCBs to strained cyclopropanes, leading to the formation of bicyclo[3.1.1]heptanes, was reported (*30*, *31*). The insertion of BCBs into heterocycles, which exist widely in nature, to forge heterobicyclic compounds has been severely curbed owing to the synthetic challenges such as activation sequence and chemo- and regioselectivity. Considering the applications of thiophenes in medicinal chemistry (*32*, *33*), we envisioned that skeletal ring enlargement of such compounds, by means of radical insertion of BCBs, would provide a privileged platform for the construction of sulfur-based bicyclic scaffolds and be a blueprint for additional efficient ring-in-a-heterocycle enlargement reactions (Fig. 1B).

This abovementioned heterocycle enlargement hypothesis would potentially operate by a cleavage-rebound sequence. A serious synthetic challenge, namely cleaving heterocycles while avoiding the ring opening of the four-membered carbocycles, requires this transformation to be carried out selectively and under mild conditions (Fig. 1B). To address this problem, a radical strategy triggered by photocatalysis can be considered, owing to its mildness and controllable character (*34*–*39*). Because of the electron-rich character and high triplet energy of thiophenes, any activation strategy making use of photoinduced energy transfer was deemed less feasible (*40*–*43*). Given that the excited-state acridinium salt {$[Acr\text{-}Mes_2]^+[BF_4]^-$}* has a high oxidation potential (*44*–*46*), it might be used as a photoredox catalyst for the precise activation of the thiophene rather than the BCB to form highly reactive radical cation intermediate **I**, which would attack the BCB and form another intermediate **II** or **III**. Then, eight-membered ring **IV** would be generated through a ring opening–insertion process, followed by the electron-transfer reduction to obtain the target molecule (Fig. 1C). Herein, a photochemical skeletal ring enlargement of thiophenes toward an array of sulfur-based bicyclic rings using BCB as an insertion unit is presented. The synthetic value, broad functional-group compatibility, and outstanding chemo- and regioselectivity of this protocol were demonstrated by scope evaluation, facile millimolar-scale synthesis and synthetic derivatization (Fig. 1D).

Reaction optimization

We began our investigation with the use of 3-phenylthiophene (**1a**) and bicyclo[1.1.0]butan-1-yl(morpholino)methanone (**2a**) as reaction partners (see supplementary materials for details; fig. S2). After optimization, product **3a** was obtained in 80% yield after reaction under argon atmosphere for 12 hours with acridinium salt as a photocatalyst and acetonitrile (MeCN) as the solvent, and good regioselectivity [**3a:3a'** = 94:6 regioselectivity ratio (r.r.)] was observed (entry 1, fig. S2). We also evaluated the effect of other reaction parameters on this skeletal ring enlargement. Varying the concentration of **1a** resulted in fluctuations in the yields but little effect on regioselectivity (entries 2 to 4, fig. S2). Moreover, changing the concentration of reaction had no effect on the yield (entries 5 and 6, fig. S2). Additionally, other solvents, such as 1,2-dichloroethane (DCE), acetone, tetrahydrofuran (THF), *N*,*N*-dimethylformamide (DMF), and benzotrifluoride ($PhCF_3$) led to a substantial decrease in the reaction yield (entries 9 to 13, fig. S2). We then investigated several photocatalysts and found that only acridinium salt could drive this chemical conversion (entries 14 to 18, fig. S2). Irradiation with visible light and the presence of photocatalyst were essential in this reaction (entries 20 and 21, fig. S2). Under the abovementioned conditions, **3a** was obtained as the predominant regioisomer over **3a'** (fig. S2). By applying a condition-based sensitivity screening approach (*47*) (Fig. 2), we found that the reaction toward compound **3a** is sensitive to high oxygen concentration and water, while being generally tolerant toward higher temperature and varying light intensities (see fig. S6 for details).

Substrate scope investigation

With the optimal conditions in hand, substrate scope with respect to the BCBs was first evaluated. As shown in Fig. 2, a series of cyclic amide–substituted BCBs proved compatible

[1]Organisch-Chemisches Institut, Westfälische Wilhelms-Universität Münster (WWU), 48149 Münster, Germany.
[2]Department of Chemistry and Biochemistry, University of California, Los Angeles, CA 90095, USA.
*Corresponding author. Email: glorius@uni-muenster.de (F.G.); houk@chem.ucla.edu (K.N.H.)
†These authors contributed equally to this work.

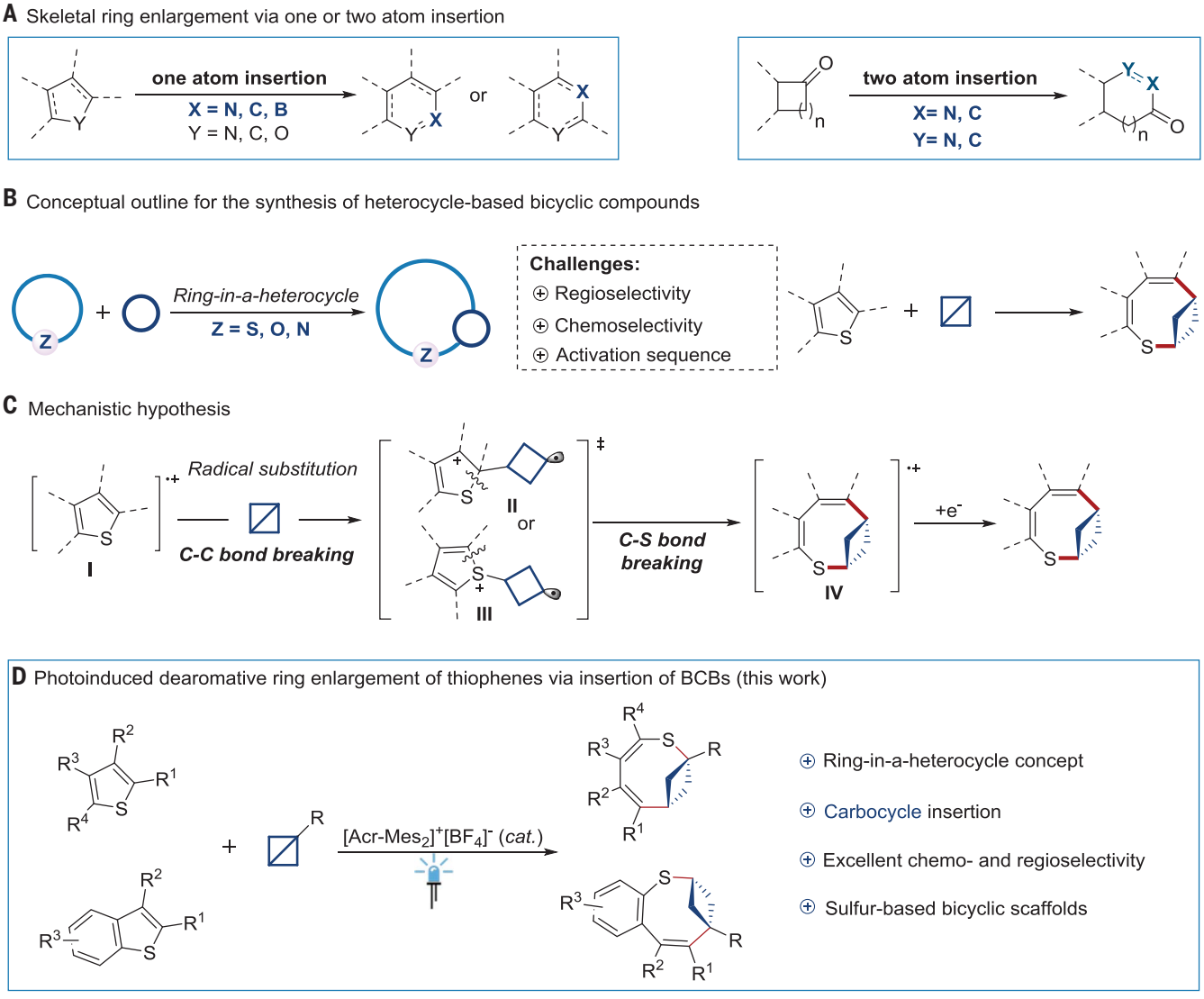

Fig. 1. Background and concept. (**A**) Skeletal ring enlargement via one- or two-atom insertion. (**B**) Conceptual outline for the synthesis of heterocycle-based bicyclic compounds. (**C**) Mechanistic hypothesis for the electron transfer–induced insertion of BCBs into thiophenes. (**D**) Photochemical skeletal ring enlargement of thiophenes through insertion of BCBs (this work). cat., catalytic.

with this transformation, affording the corresponding products in good yields and regioselectivities (**3a** to **3e**). The reaction of **1a** with **2a** was successfully performed at millimolar scale, which produced product **3a** in 84% yield. Moreover, other amide groups proved to be compatible, as shown by products **3f** to **3k**. An ester-substituted BCB reacted smoothly with **1a** to afford product **3l**. Additionally, BCBs containing ketone and ether groups gave products in a synthetically useful yield (**3m** and **3n**). Encouraged by the above results, we sought to examine the substrate scope with regard to thiophene derivatives (Fig. 2). High regioselectivities and good yields were observed with monosubstituted thiophenes as reaction partners (**3o** to **3s**). A series of functional groups on the aromatic ring, such as deuterium (**3o**), ketone (**3p**), CF_3 (**3q**), fluoride (**3r**), and chloride (**3s**), proved compatible with this protocol, providing many opportunities for further diversifications. These examples show preferential insertion proximal to the aromatic substituent. Further functional-group compatibility of this method was demonstrated with 3,4-disubstituted thiophenes as substrates (**3t** to **3w**). Reactants with aldehyde and silicon-containing ancillary groups were converted to the products **3v** and **3w**. 2,4-Disubstituted thiophenes were subsequently evaluated (**3x** to **3ac**), and higher regioselectivities were obtained than with the 3,4-disubstituted thiophenes, perhaps owing to steric hindrance. Compounds with pyridine substituents were also compatible with the reaction system (**3x** and **3y**). Thiophenes bearing an alcohol or long-chain alkyl group substitution at C2 could be transformed smoothly to the corresponding products through skeletal expansion (**3ab** and **3ac**). This conversion was successfully extended to trisubstituted thiophene, generating compound **3ad** in good yield and superb regioselectivity. Notably, methyl-substituted thiophene was compatible as well (**3ae**). Unsubstituted thiophene reacted in moderate yields to furnish the corresponding products **3af** and **3ag**. Unfortunately, no desired product was detected with the use of 2-methyl-3,5-diphenylthiophene as substrate, which might be due to the steric hindrance caused by the double substitution at the 2,5-position.

Subsequently, the substrate scope of benzothiophene derivatives was explored, and inverted regioselectivities were observed relative

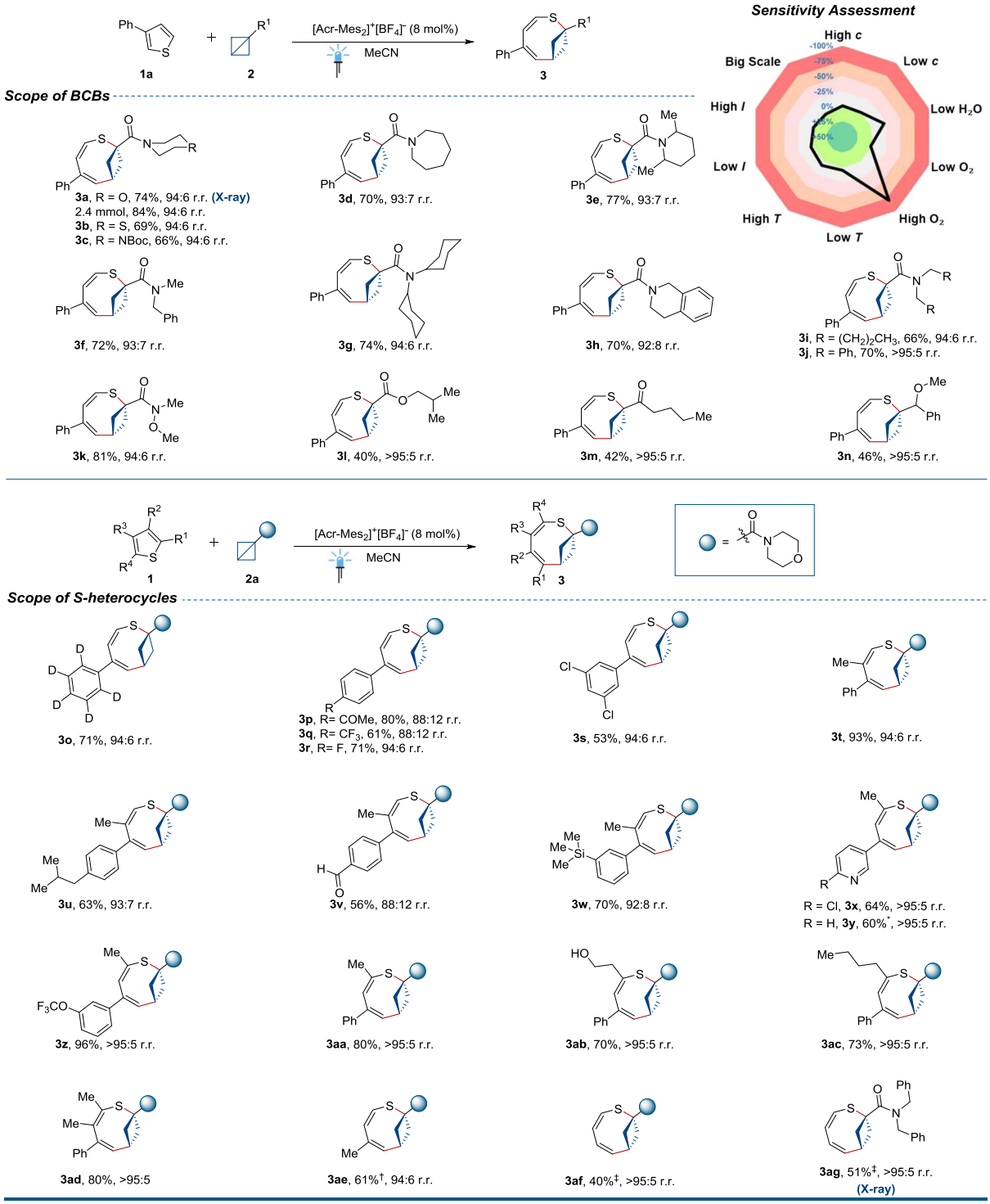

Fig. 2. Substrate scope for direct insertion of BCBs into thiophene derivatives. Yields are given for the isolated major products. Regioselectivity ratio is determined by proton nuclear magnetic resonance (^{1}H NMR) analysis of the crude product mixtures. Reaction conditions: thiophene (**1**, 0.36 mmol, 3.0 equiv), BCB (**2**, 0.12 mmol, 1.0 equiv), $[Acr\text{-}Mes_2]^+[BF_4]^-$ (8 mol %), argon, blue light-emitting diodes (LEDs; 450 nm) in MeCN (2 ml) for 12 hours at room temperature; *__1__ (4.0 equiv); †24 hours; ‡$[Acr\text{-}Mes_2]^+[BF_4]^-$ (16 mol %), **1** (4.0 equiv) for 24 hours. *c*, concentration; *T*, temperature; *I*, intensity; Ph, phenyl; Me, methyl; NBoc, *N*-*tert*-butyloxycarbonyl.

to thiophenes (Fig. 3). The target product **3ah** was obtained as a single regioisomer in 59% yield through ring-opening insertion. The robustness of this protocol was demonstrated by its compatibility with various functional groups (e.g., hydroxyl, silicon, phenyl, halogen groups) (**3ai** to **3ao**). A larger-scale reaction successfully afforded product **3ai** in 93% yield. Moreover, the scope was smoothly extended to a thiophene bearing an alkyne (**3ap**). An alkene group, which could have been reactive toward the photosensitizer, also proved compatible under standard conditions, giving product **3av**. Additionally, the cyclohexyl group was well tolerated, as shown by compound **3aq**.

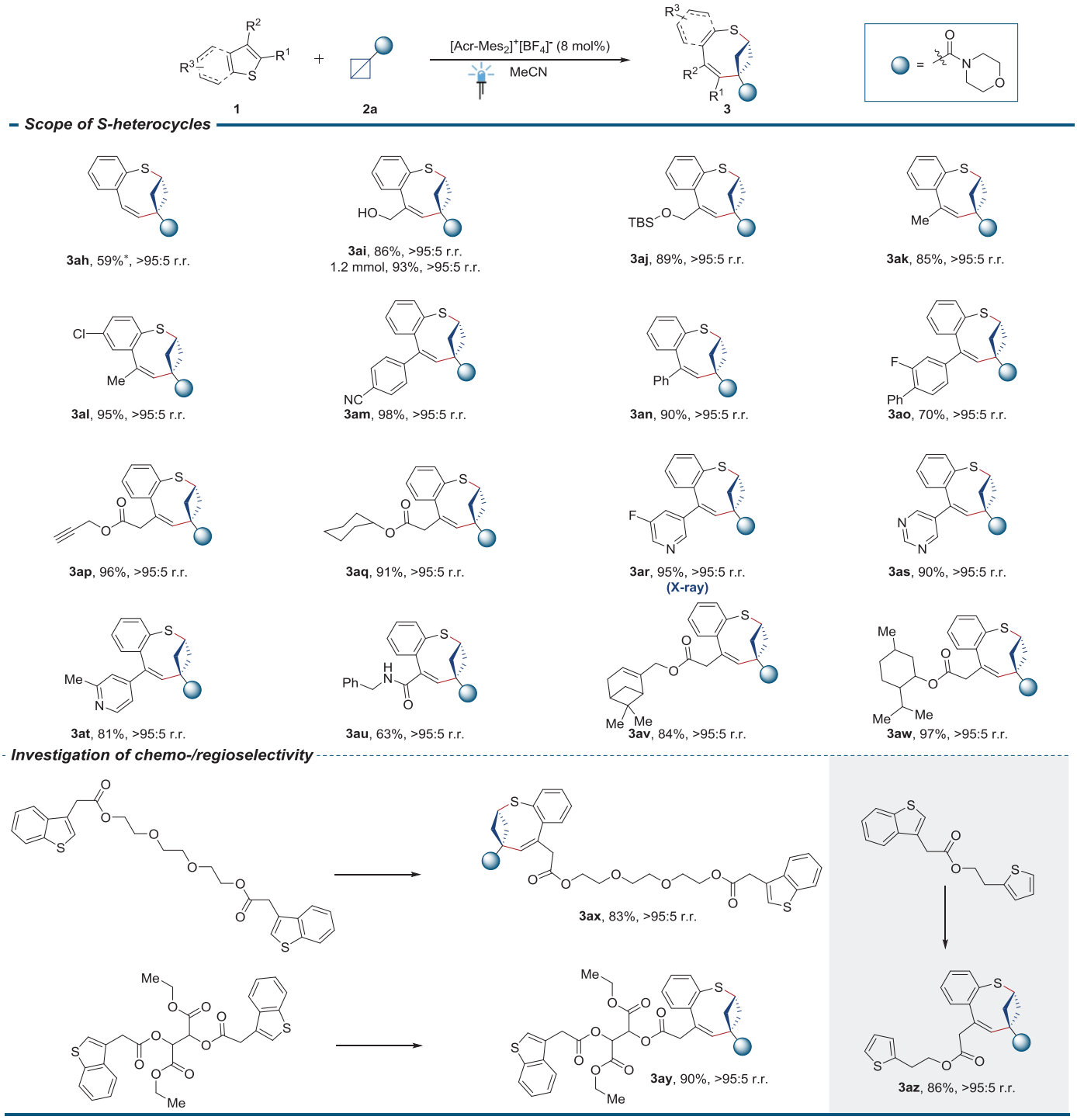

Fig. 3. Substrate scope for direct insertion of BCBs into benzothiophene derivatives. Yields are given for the isolated major products. Regioselectivity ratio is determined by ^{1}H NMR analysis of the crude product mixtures. Reaction conditions: thiophene (**1**, 0.36 mmol, 3.0 equiv), BCB (**2a**, 0.12 mmol, 1.0 equiv), $[Acr\text{-}Mes_2]^+[BF_4]^-$ (8 mol %), argon, blue LEDs (450 nm), in MeCN (2 ml) for 12 hours at room temperature; *$[Acr\text{-}Mes_2]^+[BF_4]^-$ (16 mol %), **1** (4.0 equiv) for 24 hours. TBS, *tert*-butyldimethylsilyl.

Substrates bearing pyridine and pyrimidine derivatives were amenable to this photochemical protocol, delivering corresponding products in excellent reaction yields (**3ar** to **3at**). Furthermore, benzothiophene bearing an electron-withdrawing group proved to be a suitable partner (**3au**). A substrate containing a menthol fragment was also compatible (**3aw**). To further demonstrate the chemoselectivity and regioselectivity of this heterocycle enlargement, complex molecules with two identical benzothiophene structures were treated with BCB (**2a**). Both reactions led to single-isomer products, respectively, demonstrating exceptional chemo- and regioselectivity (**3ax** and **3ay**). In a substrate with both a benzothiophene and a thiophene moiety, the BCB reacted exclusively at the benzothiophene site (**3az**). Stereochemical and

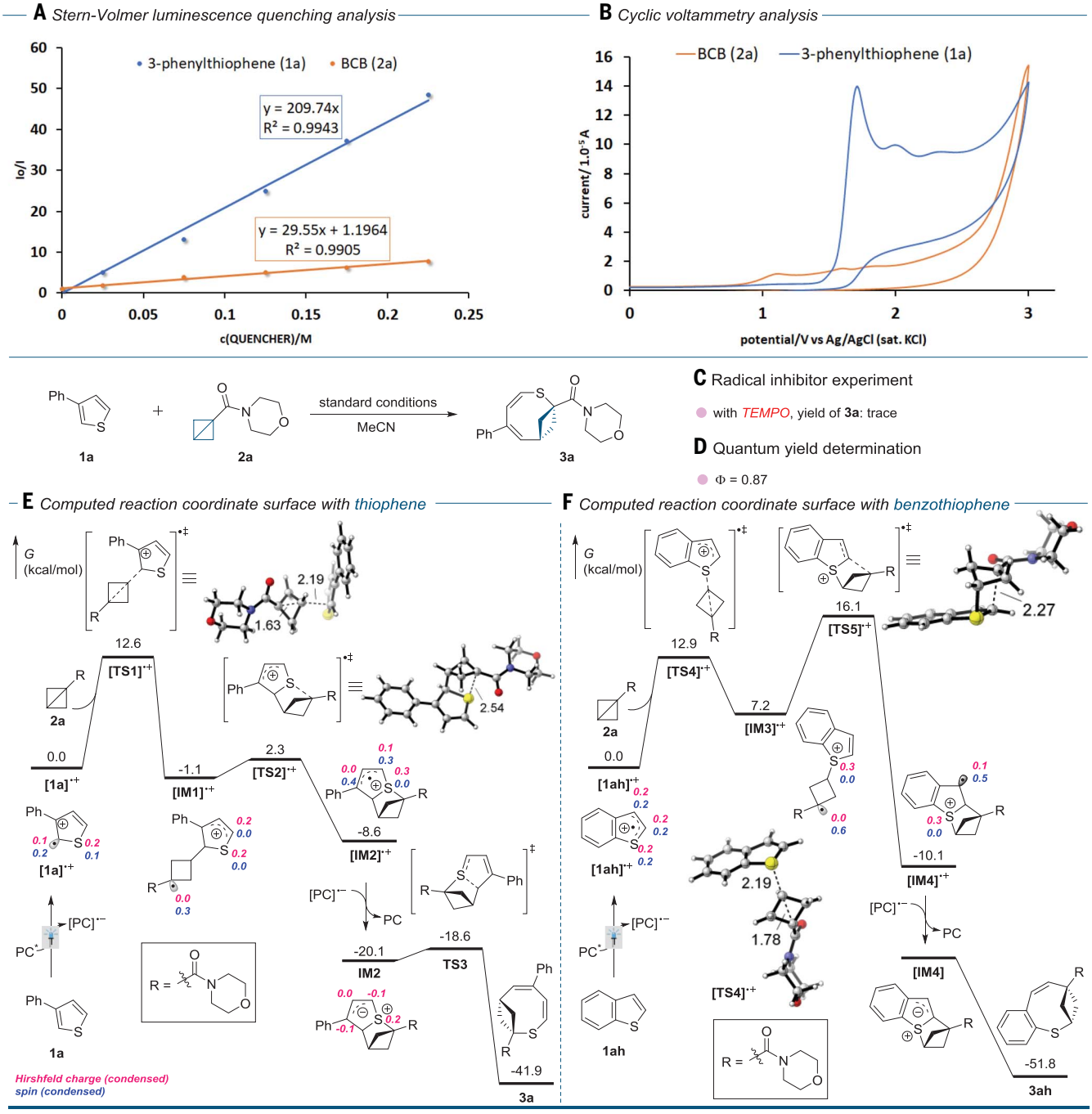

Fig. 4. Mechanistic studies. (**A**) Stern-Volmer luminescence quenching analysis. R^2, coefficient of determination. (**B**) Cyclic voltammetry analysis. (**C**) Radical inhibitor experiment. (**D**) Quantum yield determination. (**E**) Computed reaction coordinate surface with 3-phenylthiophene. (**F**) Computed reaction coordinate surface with benzothiophene. DFT calculations were conducted at the UM062X/def2TZVP/SMD(solvent = MeCN)//UM06-2X/def2SVP level of theory (*48*–*52*).

regiochemical assignments across the series of products were based on crystal structure analysis of **3a**, **3ag**, and **3ar** (CCDC 2250075-2250077).

Mechanistic investigation

We then turned our attention to the mechanism of this photoinduced ring enlargement. Stern-Volmer luminescence quenching analysis revealed that the excited-state photocatalyst (PC*) is more easily quenched by thiophene **1a** than by BCB **2a**, consistent with our original mechanistic hypothesis (Fig. 4A). Cyclic voltammetry was then performed to study the redox potentials of **1a** and **2a** (Fig. 4B). An oxidation peak of **1a** in MeCN was observed at 1.68 V [versus saturated calomel electrode (SCE)], and no oxidation peak of **2a** was detected. These results are again consistent with oxidation of **1a** but not **2a** by the PC* (oxidation potential E_{ox} = 2.00 V versus SCE) (*46*). Moreover, no desired product was generated in the presence of the radical scavenger 2,2,6,6-tetramethyl-1-piperidinyloxy (TEMPO), thereby suggesting a radical pathway (Fig. 4C). The quantum yield Φ of the reaction between **1a** with **2a** was determined to be 0.87 (Fig. 4D). Further intermolecular competition

experiments indicated that electron-rich heterocycles are more reactive than electron-poor heterocycles, selectively providing corresponding products (see supplementary materials for details).

Additionally, we performed density functional theory (DFT) calculations to gain deeper insight into the ring enlargement mechanism (Fig. 4, E and F, and figs. S9 and S10). The experimental studies suggest that the PC* oxidizes **1a** to form the radical cation intermediate [**1a**]$^{\bullet+}$. Our DFT calculation revealed the highest spin density on C2 and the highest Hirshfeld charge on the benzylic carbon, which rationalize the observed BCB insertion at C2 (Fig. 4E). The BCB insertion [**TS1**]$^{\bullet+}$ is the rate-limiting transition state with a free-energy barrier of 12.6 kcal/mol and offers the thermodynamically more stable [**IM1**]$^{\bullet+}$. Subsequent C–S bond formation to produce the heterocycle ([**TS2**]$^{\bullet+}$) is both kinetically facile and thermodynamically favored. Reduction of [**IM2**]$^{\bullet+}$ by the photocatalyst is thermodynamically favored by 11.5 kcal/mol. The final C–S bond cleavage (**TS3**) is kinetically facile, and the generation of product ***3a*** is irreversible.

Alternatively, because benzothiophene expansion takes place with inverted regioselectivity to forge ***3ah***, we hypothesized that the spin density distribution of the radical cation intermediate [**1ah**]$^{\bullet+}$ is different from that of [**1a**]$^{\bullet+}$. Indeed, our calculation showed that the spin density and Hirshfeld charges are evenly distributed over the *S*-heterocycle. Moreover, the reaction mechanism with benzothiophene (Fig. 4F) is different than that with 3-phenylthiophene (**1a**). The BCB insertion (**TS4**) into the *S*-radical has a similar free-energy barrier of 12.9 kcal/mol, as compared with **TS1**. The formation of **INT-5** is endergonic by 7.2 kcal/mol. Furthermore, the subsequent C–C bond formation is the rate-limiting transition state with a free-energy barrier of 16.1 kcal/mol. Generation of the fused heterocycle **INT-6** radical cation is exergonic by 10.1 kcal/mol. Although we could not locate the reduced [**IM4**], we expect the C–S bond cleavage to obtain the product ***3ah*** to be kinetically facile.

Product elaboration

Next, synthetic derivatization of the eight-membered sulfur-based bicyclic motifs was investigated (Fig. 5; see supplementary materials for details). Starting from compound ***3a***, aldehyde ***3ba*** was successfully produced in good yield through selective amide reduction with THF as solvent. Since sulfone and sulfoxide groups are widely used in organic synthesis, chemoselective oxidation of ***3a*** was carried out and successfully gave sulfoxide ***3bb*** and sulfone ***3bc***. Tertiary amine ***3bd*** could be produced in 64% yield through the reduction of the amide carbonyl group with the preservation of the carbon-carbon double bond. Notably, selective hydrogenation of alkene and diene within ***3a*** offered desired products ***3be*** and ***3bf*** in 76% and 87% yields, respectively, which provides more sulfur-based bicyclic compounds with different properties. Subsequently, with the use of compound ***3ai*** as a starting material, substitution with 3-bromoprop-1-ene provided allyl ether ***3bg*** by introducing an important allyl group. Compound ***3ai*** was also converted to aldehyde ***3bh*** and complex ester ***3bi*** by means of selective oxidation and esterification, respectively. These successful transformations of various functional groups further illustrate the potential applicability of these sulfur-based bicyclic motifs.

Given their wide applications in synthetic and medicinal chemistry, we used thiophene derivatives as the reaction substrates to start this ring-opening insertion protocol. Additionally, because medium-sized bicyclic scaffolds with a nitrogen and oxygen are also prevalent in both naturally occurring and synthetic bioactive molecules, we believe that this ring-in-a-heterocycle protocol will facilitate and inspire

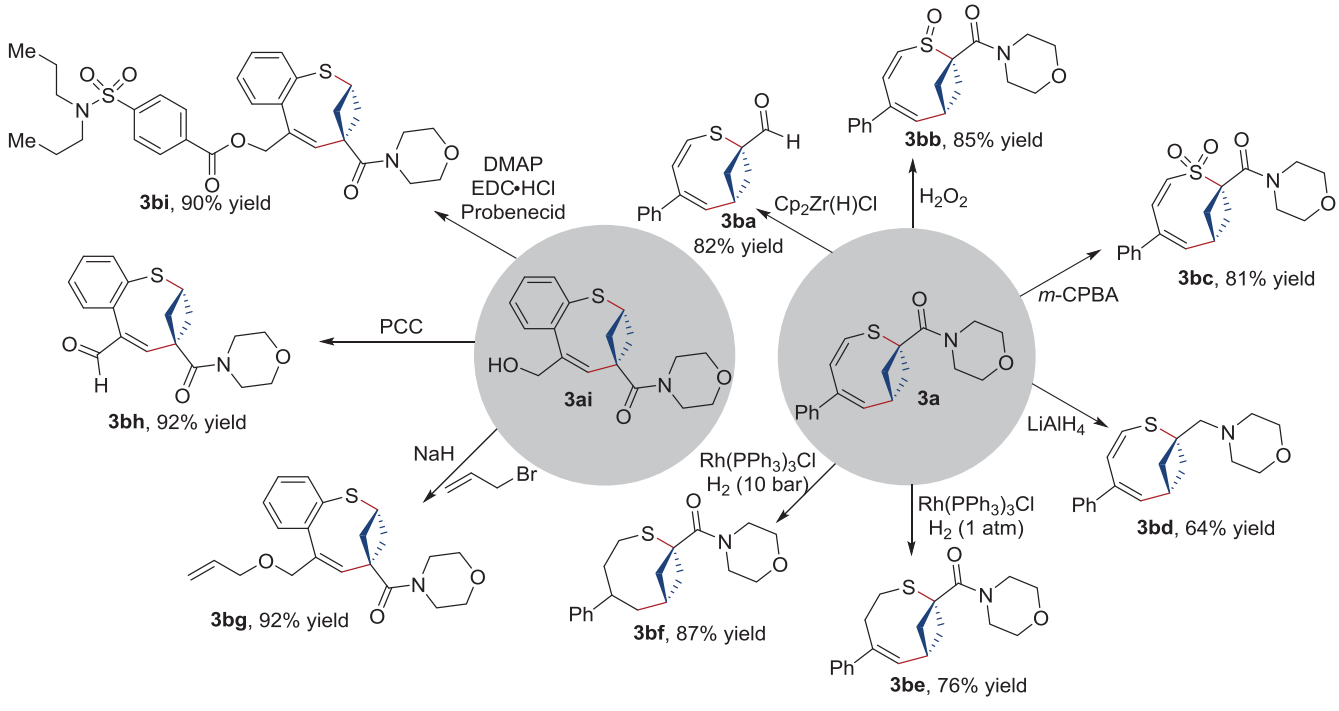

Fig. 5. Synthetic derivatization. Reaction conditions for **3ba**: $Cp_2Zr(H)Cl$ (0.2 mmol), **3a** (0.1 mmol), THF (2.5 ml); for **3bb**: H_2O_2 (0.125 mmol), **3a** (0.1 mmol), dichloromethane (DCM, 0.2 ml), trifluoroacetic acid (TFA, 0.2 ml); for **3bc**: 3-chloroperoxybenzoic acid (*m*-CPBA, 0.4 mmol), **3a** (0.1 mmol), DCM (2 ml); for **3bd**: $LiAlH_4$ (0.744 mmol), **3a** (0.1 mmol), THF (2 ml); for **3be**: $Rh(PPh_3)_3Cl$ (0.015 mmol), **3a** (0.1 mmol), H_2 (1 atm), PhMe (0.5 ml), 9 hours; for **3bf**: $Rh(PPh_3)_3Cl$ (0.015 mmol), **3a** (0.1 mmol), H_2 (10 bar), PhMe (0.5 ml), 5 hours; for **3bg**: NaH (0.096 mmol), allyl bromide (0.12 mmol), **3ai** (0.08 mmol), DMF (1.3 ml); for **3bh**: pyridinium chlorochromate (PCC, 0.15 mmol), **3ai** (0.1 mmol), DCM (0.5 ml); and for **3bi**: **3ai** (0.1 mmol), probenecid (0.12 mmol), 4-dimethylaminopyridine (DMAP, 0.12 mmol), 1-(3-dimethylaminopropyl)-3-ethylcarbodiimide hydrochloride (EDC·HCl, 0.15 mmol), DCM (0.5 ml).

the development of skeletal ring enlargements of such heterocyclic compounds through insertion of small rings.

REFERENCES AND NOTES

1. R. D. Taylor, M. MacCoss, A. D. G. Lawson, *J. Med. Chem.* **57**, 5845–5859 (2014).
2. P. D. Leeson, B. Springthorpe, *Nat. Rev. Drug Discov.* **6**, 881–890 (2007).
3. Y. Chen, C. Rosenkranz, S. Hirte, J. Kirchmair, *Nat. Prod. Rep.* **39**, 1544–1556 (2022).
4. B. Biletskyi *et al*., *Chem. Soc. Rev.* **50**, 7513–7538 (2021).
5. J. R. Donald, W. P. Unsworth, *Chem. Eur. J.* **23**, 8780–8799 (2017).
6. P. Dowd, W. Zhang, *Chem. Rev.* **93**, 2091–2115 (1993).
7. G. L. Ciamician, M. Dennstedt, *Ber. Dtsch. Chem. Ges.* **14**, 1153–1163 (1881).
8. J. Jurczyk *et al*., *Nat. Synth.* **1**, 352–364 (2022).
9. B. W. Joynson, L. T. Ball, *Helv. Chim. Acta* **106**, e202200182 (2023).
10. H. Lyu, I. Kevlishvili, X. Yu, P. Liu, G. Dong, *Science* **372**, 175–182 (2021).
11. J. C. Reisenbauer, O. Green, A. Franchino, P. Finkelstein, B. Morandi, *Science* **377**, 1104–1109 (2022).
12. J. Wang, H. Lu, Y. He, C. Jing, H. Wei, *J. Am. Chem. Soc.* **144**, 22433–22439 (2022).
13. E. E. Hyland, P. Q. Kelly, A. M. McKillop, B. D. Dherange, M. D. Levin, *J. Am. Chem. Soc.* **144**, 19258–19264 (2022).
14. Z. Wang, L. Jiang, P. Sarró, M. G. Suero, *J. Am. Chem. Soc.* **141**, 15509–15514 (2019).
15. M. Mortén, M. Hennum, T. Bonge-Hansen, *Beilstein J. Org. Chem.* **11**, 1944–1949 (2015).
16. S. Tsuchiya, H. Saito, K. Nogi, H. Yorimitsu, *Org. Lett.* **19**, 5557–5560 (2017).
17. Z. Siddiqi, W. C. Wertjes, D. Sarlah, *J. Am. Chem. Soc.* **142**, 10125–10131 (2020).
18. P. Piacentini, T. W. Bingham, D. Sarlah, *Angew. Chem. Int. Ed.* **61**, e202208014 (2022).
19. Y. Xue, G. Dong, *Acc. Chem. Res.* **55**, 2341–2354 (2022).
20. A. Trabocchi *et al*., *J. Med. Chem.* **53**, 2502–2509 (2010).
21. M. Ruiz, P. López-Alvarado, G. Giorgi, J. C. Menéndez, *Chem. Soc. Rev.* **40**, 3445–3454 (2011).
22. K. B. Wiberg, S. T. Waddell, *J. Am. Chem. Soc.* **112**, 2194–2216 (1990).
23. K. Chen, X. Huang, S. B. J. Kan, R. K. Zhang, F. H. Arnold, *Science* **360**, 71–75 (2018).
24. R. Gianatassio *et al*., *Science* **351**, 241–246 (2016).
25. X. Zhang *et al*., *Nature* **580**, 220–226 (2020).
26. W. Dong *et al*., *Nat. Chem.* **14**, 1068–1077 (2022).
27. A. Fawcett, T. Biberger, V. K. Aggarwal, *Nat. Chem.* **11**, 117–122 (2019).
28. R. Kleinmans *et al*., *Nature* **605**, 477–482 (2022).
29. S. Agasti *et al*., *Nat. Chem.* **15**, 535–541 (2023).
30. Y. Zheng *et al*., *J. Am. Chem. Soc.* **144**, 23685–23690 (2022).
31. T. Yu *et al*., *J. Am. Chem. Soc.* **145**, 4304–4310 (2023).
32. R. Shah, P. K. Verma, *Chem. Cent. J.* **12**, 137–158 (2018).
33. E. A. Ilardi, E. Vitaku, J. T. Njardarson, *J. Med. Chem.* **57**, 2832–2842 (2014).
34. C. K. Prier, D. A. Rankic, D. W. C. MacMillan, *Chem. Rev.* **113**, 5322–5363 (2013).
35. K. L. Skubi, T. R. Blum, T. P. Yoon, *Chem. Rev.* **116**, 10035–10074 (2016).
36. F. Juliá, T. Constantin, D. Leonori, *Chem. Rev.* **122**, 2292–2352 (2022).
37. N. Holmberg-Douglas, D. A. Nicewicz, *Chem. Rev.* **122**, 1925–2016 (2022).
38. M. D. Kärkäs, J. A. Porco Jr., C. R. J. Stephenson, *Chem. Rev.* **116**, 9683–9747 (2016).
39. L. Zhang, E. Meggers, *Acc. Chem. Res.* **50**, 320–330 (2017).
40. Q.-Q. Zhou, Y.-Q. Zou, L.-Q. Lu, W.-J. Xiao, *Angew. Chem. Int. Ed.* **58**, 1586–1604 (2019).
41. J. Großkopf, T. Kratz, T. Rigotti, T. Bach, *Chem. Rev.* **122**, 1626–1653 (2022).
42. F. Strieth-Kalthoff, M. J. James, M. Teders, L. Pitzer, F. Glorius, *Chem. Soc. Rev.* **47**, 7190–7202 (2018).
43. W. M. Flicker, O. A. Mosher, A. Kuppermann, *Chem. Phys. Lett.* **38**, 489–492 (1976).
44. I. A. MacKenzie *et al*., *Nature* **580**, 76–80 (2020).
45. C. Song *et al*., *Angew. Chem. Int. Ed.* **58**, 12206–12210 (2019).
46. L. Pitzer, F. Sandfort, F. Strieth-Kalthoff, F. Glorius, *Angew. Chem. Int. Ed.* **57**, 16219–16223 (2018).
47. L. Pitzer, F. Schäfers, F. Glorius, *Angew. Chem. Int. Ed.* **58**, 8572–8576 (2019).
48. Y. Zhao, D. G. Truhlar, *Theor. Chem. Acc.* **120**, 215–241 (2008).
49. F. Weigend, R. Ahlrichs, *Phys. Chem. Chem. Phys.* **7**, 3297–3305 (2005).
50. A. V. Marenich, C. J. Cramer, D. G. Truhlar, *J. Phys. Chem. B* **113**, 6378–6396 (2009).
51. G. Luchini, J. V. Alegre-Requena, I. Funes-Ardoiz, R. S. Paton, *F1000 Res.* **9**, 291–304 (2020).
52. M. J. Frisch *et al*., Gaussian 16 Revision C.01 (Gaussian Inc., 2016).

ACKNOWLEDGMENTS

We thank Y. Li (Wuhan University) and R. Mayska, P. Bellotti, and J. E. Erchinger (WWU) for assistance and discussions. **Funding:** Generous financial support was provided by the Alexander von Humboldt Foundation (H.W.), the Deutsche Forschungsgemeinschaft (Leibniz Award), and the International Graduate School for Battery Chemistry, Characterization, Analysis, Recycling and Application (BACCARA). This work was also funded by the Ministry for Culture and Science of North Rhine Westphalia, Germany (A.D.). DFT calculations were performed on the IDRE Hoffman2 cluster at the University of California, Los Angeles, and the Extreme Science and Engineering Discovery Environment (XSEDE), which is supported by the National Science Foundation (OCI1053575). Additional funding was provided to K.N.H. by the NSF (CHE-2153972). **Author contributions:** F.G. and H.W. conceived of the project. H.W., A.D., and S.D. designed and conducted experiments. K.N.H., H.S., and H.T.C. conducted the computational studies. C.D. analyzed the x-ray structures. H.W., H.S., K.N.H., and F.G. supervised the research and wrote the manuscript, with contributions from all authors. **Competing interests:** The authors declare no competing interests. **Data and materials availability:** The Cambridge Crystallographic Data Centre (CCDC) website contains the supplementary crystallographic data for this paper, which can be obtained free of charge at www.ccdc.cam.ac.uk/ data_request/cif under identifiers 2250075, 2250076, and 2250077. All other data are available in the supplementary materials.

SUPPLEMENTARY MATERIALS

science.org/doi/10.1126/science.adh9737
Materials and Methods
Supplementary Text
Figs. S1 to S10
X-Ray Data
NMR Spectra
References (*53*–*73*)

Submitted 26 March 2023; accepted 30 May 2023
10.1126/science.adh9737